Penson-Kolb-Hubbard model: A study of the competition between single-particle and pair hopping in one dimension

Achille Hui
Department of Physics, Stanford University, Stanford, California 94305

S. Doniach
Department of Applied Physics, Stanford University, Stanford, California 94305
(Received 21 January 1993)

In this paper, we present a study of the ground-state phase diagram of a one-dimensional quantum chain, the Penson-Kolb-Hubbard model,

$$H=-\sum_{i,\eta=\pm1,\sigma}(tc^{\dagger}_{i+\eta\sigma}c_{i\sigma}+Vc^{\dagger}_{i+\eta\uparrow}c^{\dagger}_{i+\eta\downarrow}c_{i\downarrow}c_{i\uparrow})+\sum_i Un_{i\uparrow}n_{i\downarrow}$$

at half filling. We have examined the system using exact diagonalization for samples of up to 12 sites and employed two techniques, eigenprojection decomposition and twisted-boundary conditions, in analyzing the data. These techniques allow us to characterize the ground state in a manner insensitive to changes in sample size and provide us with a clean way to visualize the physics. When used with the "correct" order parameter, qualitative features emerge even for sample sizes as small as six sites. We find that the second-order charge-density-wave–spin-density-wave transition in the weak-coupling limit ($t \gg U \sim 2V$) turns into a first-order superconducting–antiferromagnetic transition in the strong-coupling regime [$t \ll U \sim (4/\pi)V$]. We also observe evidence of a charge-density-wave–superconducting transition in the parameter range ($t \sim V \gg U$). These three transition lines meet together at a tricritical point at ($t:U:V$)$\sim$(0.04:0.54:0.42). A naive renormalization-group analysis in the intermediate-coupling regime produces results consistent with this conclusion.

I. INTRODUCTION

There are two facts that make the proposed Penson-Kolb-Hubbard (PKH) model

$$H=-\sum_{i,\eta=\pm1,\sigma}(tc^{\dagger}_{i+\eta\sigma}c_{i\sigma}+Vc^{\dagger}_{i+\eta\uparrow}c^{\dagger}_{i+\eta\downarrow}c_{i\downarrow}c_{i\uparrow})+\sum_i Un_{i\uparrow}n_{i\downarrow}$$

an interesting object to study. First, many of the high-T_c materials discovered within the past few years, in particular the cuprates, share certain common characteristics. For example, the "Cooper" pairs observed are extremely small with coherence lengths comparable with the size of the unit cell. The on-site electron-electron repulsion U is notably stronger than the single-particle hopping amplitude t. Finally, the undoped materials are insulators and superconductivity is triggered by changes in doping.

It is generally accepted that the insulating behavior of undoped materials is caused by the strong on-site electron-electron repulsion and that some sort of Hubbard model will adequately describe the physics of the insulating phase. In this paper we assume that when the materials are doped, some unexplained mechanism binds pairs of charged carriers tightly together and that the resulting "Cooper" pairs move freely as single entities in equilibrium with single carriers. We assume that the physics of the doped materials can then be modeled through a suitable choice of effective interactions among the pairs. Since the Penson-Kolb-Hubbard model captures many of these phenomenological characteristics, we can use it to study some of the possible phases of high-T_c materials.

Penson and Kolb[1] introduced their one-dimensional *pair-hopping model*, our PKH model without the Hubbard-U term, as a model for electron segregation. They found that a single-particle excitation gap, ΔE_{single}, opens up when the pair-hopping amplitude V increases beyond $\sim 1.4t$. This is not very surprising because the model is superconducting in the infinite-V limit by construction. What is surprising is that the second-order derivative of ground-state energy E with respect to V, d^2E/dV^2—the analog of specific heat, shows a local maximum at $V \sim 1.4t$ which neither diverges nor disappears on extrapolation to the infinite sample-size limit. Using this and some other scaling arguments, Penson and Kolb inferred the existence of a transition of the model at $V \sim 1.4t$ which is neither first nor second order.[1] Affleck and Marston restudied this problem using renormalization-group equations. In the weakly coupled continuum limit, they found that the pair-hopping model and the negative-U Hubbard model are essentially equivalent. The only differences are in the values of the bare coupling constants, so that this places the two models in the same region of the phase diagram.[2] As a result, they suggested that the apparent transition at $V \sim 1.4t$ could be just a finite-size artifact. This leads us to ask the question whether there really is a transition and if so, what is the nature of this transition.

0163-1829/93/48(4)/2063(11)/$06.00

In this paper we will restrict ourselves to the study of the one-dimensional PKH model with non-negative t, U, V. The restriction of $t \geq 0$ is purely a convenience. This is because under the canonical transform $c_{i\sigma}^{\dagger} \rightarrow (-1)^i c_{i\sigma}^{\dagger}$, the t term of the PKH Hamiltonian simply changes sign. The one-dimensional and non-negative V restrictions are motivated by our desire to compare with Penson and Kolb's result.[1] In addition, we believe that if we approximate the physics of the cuprates by the PKH model, the relevant V should be non-negative in the superconducting phase and U has to be non-negative in the insulating phase. In the following sections we first justify our choice of Hamiltonian. Then based on heuristic arguments, we explain what we should expect for the phase diagram of the one-dimensional PKH model. We present numerical evidence supporting our predictions. Finally, we compare our numerical results with predictions based on renormalization-group analysis and discuss briefly the deviations of our results from Affleck and Marston's analysis.[2]

II. CONSTRUCTION OF THE PKH MODEL

A. Physical justification

If we perturb the one-dimensional Hubbard model to favor the formation of "small" pairs, the pairs formed will "block" the hopping of normal unpaired particles due to the Pauli-exclusion principle. In the dilute "pair" limit, the physics should be dominated by this type of competition between single particle and localized pair hopping instead of interactions among the pairs. As a result, the role of the pairs should be expressible as an interaction term quadratic in the pair creation $\Delta_i^{\dagger} = c_{i\uparrow}^{\dagger} c_{i\downarrow}^{\dagger}$ and annihilation $\Delta_i = c_{i\downarrow} c_{i\uparrow}$ operators,

$$H_{\text{pair}} = \sum_{i,\eta,\sigma} V_\eta \Delta_{i+\eta}^{\dagger} \Delta_i$$

$$= \sum_i V_0 n_{i\uparrow} n_{i\downarrow} + \sum_{i,\eta=\pm1,\pm2,\ldots,\sigma} V_\eta \Delta_{i+\eta}^{\dagger} \Delta_i \ .$$

The term V_0 and V_η ($\eta = \pm1, \pm2, \ldots$) represent the pairs' potential and kinetic energies, respectively. Physically, we expect $|V_{\pm1}| \geq |V_{\pm2}| \geq \cdots$, and the Fourier transform $\tilde{V}_k$ to be a real, even function of k. In addition, $\tilde{V}_{|k|}$ should be monotonically increasing for $0 < |k| < \pi$. As a result, it just suffices to keep the $U := V_0$ and $V := -V_1$ terms to get the right qualitative shape of $\tilde{V}_k$. Similarly, we can restrict single-particle hopping only to nearest neighbor and arrive at

$$H = -\sum_{i,\eta=\pm1} \left[t \sum_\sigma c_{i+\eta\sigma}^{\dagger} c_{i\sigma} + V \Delta_{i+\eta}^{\dagger} \Delta_i \right]$$

$$+ U \sum_i n_{i\uparrow} n_{i\downarrow} - \mu \sum_{i,\sigma} n_{i,\sigma} \ .$$

We will restrict our study to the case of half filling. For the sample sizes we have used in our calculation, we believe they are simply too small to make any meaningful statement for doping away from half filling. However, we would like to argue that in the intermediate- and strong-coupling regime ($U, V \gtrsim t$) the qualitative features of the phase diagram will not depend on our specific choice of half filling. This is because as we increase the couplings, momentum states far away from the Fermi surface become energetically accessible. Unlike the case of a weakly interacting Fermi gas, we no longer require to fulfill the "perfect nesting" condition in order to have a charge-density-wave phase. We hypothesize that when we dope the materials, the main effects of the pairs will be captured by the effective interaction among the pairs themselves so that it is no longer necessary to consider the doping dependence explicitly in the medium-strong-coupling part of the phase diagram.

At half filling, particle-hole symmetry forces $\mu = U/2$ independent of t and V. The chemical-potential term $-\mu \sum_{i,\sigma} n_{i,\sigma}$ becomes irrelevant in the determination of the ground state and we will simply drop it in the following discussion.

B. Heuristic expectations based on various known limits

We are left with two dimensionless parameters U/t and V/t. As we have discussed in Sec. II A, we will restrict ourselves to the parameter space where both of them are non-negative. Using the fact that simultaneous scaling of all three parameters t, U, V leaves the ground state invariant, we can represent the phase diagram by an equilateral triangle tUV as shown in Fig. 1. Figure 1 summarize all the important results of this paper. The

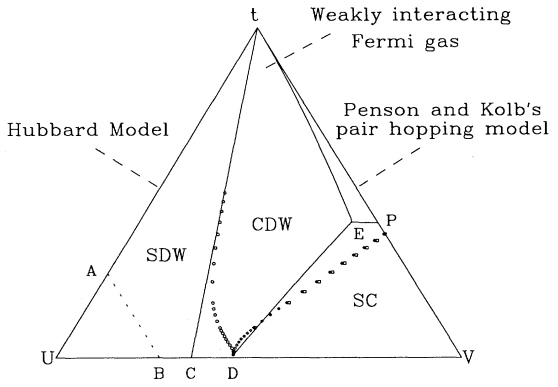

FIG. 1. An equilateral triangle representing the parameter space $t + U + V = 1$ of the Penson-Kolb-Hubbard model. Any point p inside the triangle tUV corresponds to

$$t : U : V = \text{dist}(p, UV) : \text{dist}(p, tV) : \text{dist}(p, tU) \ ,$$

where dist(p, AB) is the distance between the point p and the line segments AB. The solid lines tC, tE, EP, and DE are phase boundaries predicted by renormalization-group equations Eqs. (4.2a)–(4.2d) using initial conditions Eqs. (4.1a)–(4.1d) at cutoff $\delta = 0.02$ while the dashed line AB is supposed to be an artifact. The circles represent the CDW-SDW transition line we located by maximizing $(N/t)|E_{K=0}(\phi_s = \pi) - E_{K=0}(\phi_s = 0)|$ for $N = 10$. The diamonds and squares are the CDW-SC transition line we estimated by minimizing the expression $\frac{1}{6}\sum_\lambda [P_{O_{\text{CDW}}}(\lambda+1) - 2P_{O_{\text{CDW}}}(\lambda) + P_{O_{\text{CDW}}}(\lambda-1)]^2$ for $N = 10$ and 12, respectively.

boundaries of the triangle represents various known limits we will describe here. We will defer the discussion of other details of Fig. 1 to the relevant sections.

Along the tU line where $V=0$, the model reduces to the one-dimensional Hubbard model[3] which is exactly solvable. It is well known that at half filling, there is a gap ΔE_ρ ($\sim e^{-\text{const}\, t/U}$ for small U) in the charge sector but none in the spin sector. As U varies, the ground state depends on U analytically and hence no transition is possible along the tU line.

Around the vertex t where $t \gg U \sim V$, the model is nothing but the usual one-dimensional weakly interacting fermion gas. If we take the continuum limit naively, our model will be equivalent to the Hubbard model with the Hubbard-U replaced by $U-2V$. As a result, we should expect a charge-density-wave–spin-density-wave (CDW-SDW) transition line at $U \sim 2V$ (tC in Fig. 1).

Along the tV line, the model reduces to Penson and Kolb's pair-hopping model. Penson and Kolb's study suggests that there may be a transition at $V \sim 1.4t$ (P in Fig. 1) and Affleck and Marston's study shows that, at least in the weak-coupling limit, there is a gap ΔE_s ($\sim e^{-\text{const}\, t/2V}$ for small V) in the spin sector but none in the charge sector.

Along the UV line where $t=0$, the parity of the number of particles at each site is a good quantum number. This allows us to decompose the eigenspace of H into sectors specified by the parity of the occupation number at each site. Within any sector, the system is a collection of "even" segments, within which pairs are confined, interleaved with immobile "odd" sites. We can apply the Jordan-Wigner transform on each even segment and trivially solve the model. We find that for small U, the ground state is nondegenerate and consists of a single infinitely long even segment with freely moving pairs. As we increase U, a first-order transition will occur at $U=(4/\pi)V$ ($\sim D$ in Fig. 1). Above this value, the ground state is infinitely degenerate. All sites are singly occupied and the spins of all particles are independent of each other. There is a gap $\propto U-(4/\pi)V$ for pair formation, and the V term becomes irrelevant to the physics. As a result, the model reduces to the Hubbard model in the parameter range $t \ll (4/\pi)V \lesssim U$ and the system is basically an antiferromagnetic insulator.

Combining the information along the boundaries of the triangle tUV, we expect the second-order CDW-SDW transition in the weak-coupling limit ($t \gg U \sim 2V$) changes to a first-order superconducting (SC)–antiferromagnetic (AF) transition in the strong-coupling regime [$t \ll U \sim (4/\pi)V$]. There will also be a CDW-SC transition line at ($t \sim V \gg U$) and these three transitions lines will meet at a tricritical point within the triangle. This is indeed what we find when we exactly diagonalize the Hamiltonian for small systems.

III. ANALYSIS BASED ON EXACT DIAGONALIZATION

Initially, we tried to attack the problem by studying the single-particle and pair excitation gaps defined by

$$\Delta E_{\text{single}} := \tfrac{1}{2}(E_{N,m+1,m} + E_{N,m-1,m} - 2E_{N,m,m}) ,$$

$$\Delta E_{\text{pair}} := \tfrac{1}{2}(E_{N,m+1,m+1} + E_{N,m-1,m-1} - 2E_{N,m,m}) ,$$

where $E_{N,m,n}$ is the ground-state energy for a system of N sites with m spin-up and n spin-down electrons, using exact diagonalization based on the *Lanczos algorithm*[4] augmented by finite-size scaling analysis. Figure 2 shows the scaled energy gaps we obtained along the tV line ($U=0, V=1, m=N/2, N=6,8,10$). It clearly shows that while the scaled pair excitation gap $N\Delta E_{\text{pair}}$ remains finite for all t/V, the scaled single-particle gap $N\Delta E_{\text{single}}$ diverges for $t/V \leq 0.7$. This is consistent with Penson and Kolb's result of the opening of a single-particle excitation gap at $t/V \sim 0.7$

However, it is apparent that the energy gaps in these graphs exhibit a sample-size dependence of period 4. This is also true for other numerical data we have collected. For any one-dimensional numerical calculation, $N=6$ is about the minimum size for which we could trust the result. This implies we need calculations on systems of 14 sites in order to make a $1/N$ interpolation. This makes finite-size scaling analysis unattractive. From the numerical data we have collected, we also notice that the ground-state energies and energy gaps offer no distinct features as we vary the parameters (t, U, V) over the interior of the tUV triangle. As a result, we found that we needed more sensitive tools to characterize the physics in different regions of the phase space. Here we report on two techniques which proved useful in helping us study the ground-state phase diagram.

A. Eigenprojection decomposition

The first technique was introduced by Cannon, Scalettar, and Fradkin in Ref. 5. Given any physical system which exhibits a phase transition when its parameters are varied, let O be the order parameter, $\hat{O}$ the corresponding operator, and $|\Psi_0\rangle$ the ground state. Instead of looking at the ground-state correlation functions, we can perform

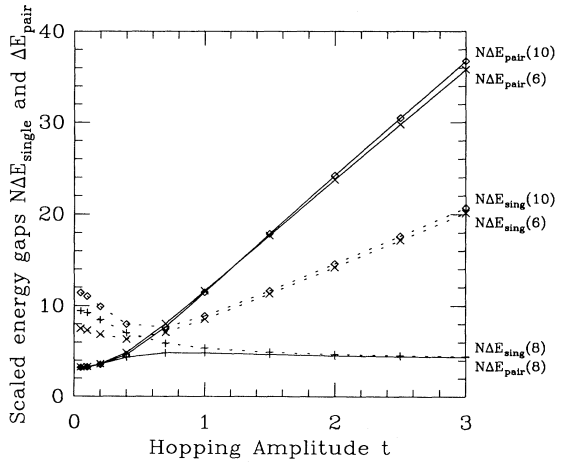

FIG. 2. The scaled single-particle and pair excitation gaps $N\Delta E_{\text{single}}$ and $N\Delta E_{\text{pair}}$ for various single-particle hopping amplitude t ($0.05 \leq t \leq 3.0$) and sample sizes $N=6,8,10$ at $U=0.0, V=1.0$.

a spectral decomposition of $\hat{O}$ and look at the ground-state expectation values of its eigenprojection operators

$$\hat{P}_{\hat{O}}(\lambda_i)=\sum_j |\phi_{\lambda_i,j}\rangle\langle\phi_{\lambda_i,j}| ,$$

where $\phi_{\lambda_i,j}$ is a complete set of states of $\hat{O}$'s eigenstate space $\mathcal{V}_{\lambda_i}$ associated with eigenvalue λ_i. We have the following decompositions:

$$\hat{O}=\sum_i \lambda_i \hat{P}_{\hat{O}}(\lambda_i) ,$$

$$O=\langle\Psi_0|\hat{O}|\Psi_0\rangle=\sum_i \lambda_i \langle\Psi_0|\hat{P}_{\hat{O}}(\lambda_i)|\Psi_0\rangle$$

$$=\sum_i \lambda_i P_O(\lambda_i) .$$

We can interpret $P_O(\lambda_i)$ as the probability that $O=\lambda_i$ in the ground state. Therefore, the function $P_O(\lambda)$ can be viewed as the exponential of a Ginzburg-Landau functional associated with the order parameter O. With this identification in mind, one can infer the order of the transition, as demonstrated in Ref. 5, from the dependence of $P_O(\lambda)$ upon its parameters.

We apply this technique to the exact eigenvectors generated by the Lanczos algorithm[6] for the charge-density-wave order parameter, $\hat{O}_{\rm CDW}=\sum_{i,\sigma}(-1)^i n_{i,\sigma}$, as well as the superconducting order parameter $\hat{O}_{\rm SC}=\Delta^\dagger=\sum_i \Delta_i^\dagger=\sum_i c_{i\uparrow}^\dagger c_{i\downarrow}^\dagger$. Unlike $\hat{O}_{\rm CDW}$, the spectral decomposition of $\hat{O}_{\rm SC}$ is a little bit tricky. First, it is not a Hermitian operator. We can circumvent this by studying its real/or imaginary part. Second, $\hat{O}_{\rm SC}$ does not preserve fermion number and hence $\langle\Psi_0|\hat{O}_{\rm SC}|\Psi_0\rangle\equiv 0$. As a result, we cannot evaluate the desired $P_{{\rm Re}(O_{\rm SC})}$ directly using the ground-state vectors we generated through the Lanczos algorithm.[7] However, since $\Delta^\dagger,\Delta$, and $\Delta_z=\frac{1}{2}\sum_i(n_{i\uparrow}+n_{i\downarrow}-1)$ form a spin algebra, and Δ_z commutes with H, we can study the spectral decomposition of $|\Delta|^2=\frac{1}{2}(\Delta^\dagger\Delta+\Delta\Delta^\dagger)+\Delta_z^2$ instead.

Consider $|\psi_{\lambda(\lambda+1)}\rangle$, the projection of $|\Psi_0\rangle$ to the eigensubspace $\mathcal{V}_{\lambda(\lambda+1)}$ of $|\Delta|^2$. We have $\Delta_z|\psi_{\lambda(\lambda+1)}\rangle\equiv 0$ at half filling. From group theory, we know this relation will allow us to determine its projection onto any eigenstate of ${\rm Re}(\hat{O}_{\rm SC})$ in $\mathcal{V}_{\lambda(\lambda+1)}$ uniquely. As a result, $P_{{\rm Re}(O_{\rm SC})}$ can be expressed in terms of $P_{|\Delta|^2}$,

$$P_{{\rm Re}(O_{\rm SC})}(m)=\sum_i \langle\Psi_0|\phi_i(m)\rangle\langle\phi_i(m)|\Psi_0\rangle=\sum_{i\lambda}\langle\psi_{\lambda(\lambda+1)}|\phi_i(m)\rangle\langle\phi_i(m)|\psi_{\lambda(\lambda+1)}\rangle$$

$$=\sum_\lambda |(\lambda,j_z=0|\lambda,j_x=m)|^2\langle\psi_{\lambda(\lambda+1)}|\psi_{\lambda(\lambda+1)}\rangle$$

$$=\sum_{k=0,1,\ldots}\frac{(2k)!(2|m|+2k)!}{4^{|m|+2k}k!^2(|m|+k)!^2}P_{|\Delta|^2}((|m|+2k)(|m|+2k+1)) ,$$

where $\phi_i(m)$ form a complete set of states for the ${\rm Re}(\hat{O}_{\rm SC})=m$ eigensubspace and $|\lambda,m)$ are basic vectors for the spin-λ irreducible representation of SU(2). Therefore, we will only consider $P_{|\Delta|^2}(\lambda(\lambda+1))$ in the following discussion.

In Fig. 3 we have plotted $P_{|\Delta|^2}(\lambda(\lambda+1))$ vs (λ,U) along a line parallel to UV at $t=0.01$ for $0.2\le U\le 0.8$, $U+V=1.0$, $N=10$. It is clear that when U increases beyond 0.57, the functional form of $P_{|\Delta|^2}(\lambda(\lambda+1))$ changes drastically. When $U/(U+V)<0.57$, $P_{|\Delta|^2}(\lambda(\lambda+1))$ is nearly zero for all $\lambda=N/2-1,N/2-3,\ldots$ and dominated by $\lambda=\lambda_{\max}=N/2$. In contrast, when $U/(U+V)>0.57$, $P_{|\Delta|^2}(\lambda(\lambda+1))$ is completely dominated by its $\lambda=0$ component. This implies the system is superconducting for $U/(U+V)<0.57$ and that superconductivity disappears at $U/(U+V)\sim 0.57$. The drastic differences in the shape of $P_{|\Delta|^2}(\lambda(\lambda+1))$ for $U/(U+V)<0.57$ and >0.57 signify a first-order transition.

In Fig. 4 we have plotted the corresponding results at $t=0.1$. The functional form of $P_{|\Delta|^2}(\lambda(\lambda+1))$ no longer changes discontinuously as we increase U. Indeed, as we

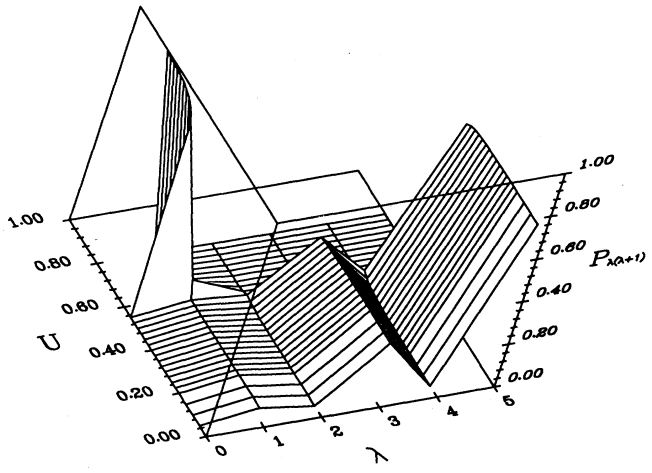

FIG. 3. The ten-site eigenprojection decomposition $P_{|\Delta|^2}(\lambda(\lambda+1))$ of the square modulus of superconducting order parameter $|\Delta|^2$ for various U $(0.05\le U\le 0.8, V=1.0-U)$ at $t=0.01$. The drastic change in the qualitative shape of $P_{|\Delta|^2}(\lambda(\lambda+1))$ at $U\sim 0.57$ signifies a first-order transition.

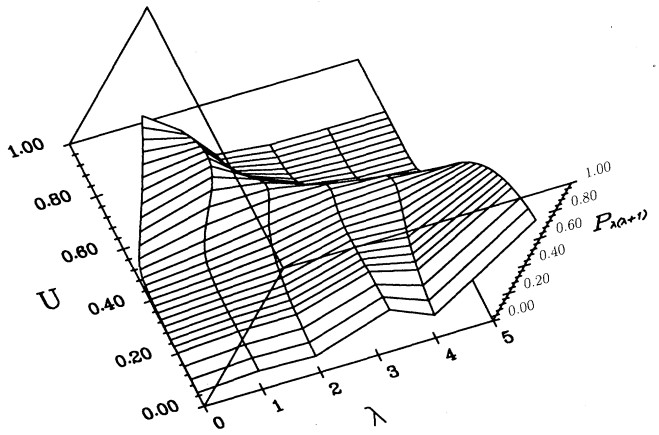

FIG. 4. Same plot as Fig. 3 at $t=0.10$. The drastic change of the qualitative shape of $P_{|\Delta|^2}(\lambda(\lambda+1))$ at $U\sim 0.57$ has been completely smoothed out. This implies the transition has been switched to a second-order one.

increase U, the peak of $P_{|\Delta|^2}(\lambda(\lambda+1))$ moves from $\lambda_{\max}$ to 0 smoothly, signifying a second-order transition.

In Fig. 5(a) we have plotted $P_{|\Delta|^2}((\lambda+1))$ for odd λ at $t=0.04$, $N=10$. Pay attention to the little bump for $\lambda=1$ at $U/(U+V)\sim 0.57$. For $t=0.03$, this bump is relatively sharp and it smoothes out when $t=0.05$. In Fig. 5(b) we have plotted $P_{O_{\rm CDW}}(\lambda)=\langle\Psi_0|\hat{P}_{\hat{O}_{\rm CDW}}|\Psi_0\rangle$ at $t=0.04$, $N=8$. Once again, the cusp of $P_{O_{\rm CDW}}(0)$ at $U/(U+V)\sim 0.57$ is relatively sharp at $t=0.03$ and smoothes out when $t=0.05$. From this, we estimate that at $t/(U+V)=0.04\pm 0.01$, the first-order transition for small t changes to a second-order transition at larger t.

In Fig. 6 we have plotted $P_{O_{\rm CDW}}(\lambda)$ for $t=0.01$, 0.1, 0.4, and 0.7, $N=8$. There are several notable features. First, $\partial P_{O_{\rm CDW}}(0)/\partial U$ has a discontinuity at $U/(U+V)\sim 0.6\pm 0.05$. This point seems to move toward bigger U as we increase t and there is an obvious change of shape of $P_{O_{\rm CDW}}(\lambda)$ when $U/(U+V)$ increases beyond this value. Second, for small t, $P_{O_{\rm CDW}}(\lambda)$ in the small-U side shows extremely strong even-odd dependence on λ. As we increase t, this even-odd dependence in $P_{O_{\rm CDW}}$ diminishes. The boundary that separates the regions with and without such dependence seems to move towards the tV line and completely go away at $t/(U+V)\sim 0.7$. This suggests that there are actually two second-order transition lines when we increase $t/(U+V)$ beyond ~ 0.05. As we increase t further, one of them moves slowly toward the asymptote $U/(U+V)\sim 0.67$ while the other towards the tV line and completely goes away at a place consistent with Penson and Kolb's assignment of a transition point.

B. Twisted boundary conditions

A second technique to identify phase transitions originates from the study of the helicity modulus in a superfluid. In a superfluid, if we apply a gauge transformation $\rho\rightarrow e^{i\phi}\rho$ to the superfluid order parameter ρ,[8] the free energy F of the system will acquire an extra term proportional to ρ and $|\nabla\phi|^2$: $F\rightarrow F+\text{const}\,\rho|\nabla\phi|^2$. As a result, if we perform a finite-size calculation on a superfluid system contained in a volume of length scale L using a twisted boundary condition $\rho(x+L)=e^{i\phi}\rho(x)$, the ground-state energy E_0 of the system will have a ϕ dependence of the form $\text{const}\,\rho(\phi^2/L)$ and hence we can use E_0 with different boundary conditions to extract the superfluid order parameter ρ.

We have implemented this idea into our numerical calculation by "twisting" the boundary condition. We have considered two classes of boundary conditions,

$$\text{pair twist:}\quad c^{\dagger}_{i+N,\sigma}=e^{i\phi_p}c^{\dagger}_{i,\sigma}\ , \tag{3.1a}$$

$$\text{spin twist:}\quad c^{\dagger}_{i+N,\sigma}=e^{i\phi_s\sigma}c^{\dagger}_{i,\sigma}\ . \tag{3.1b}$$

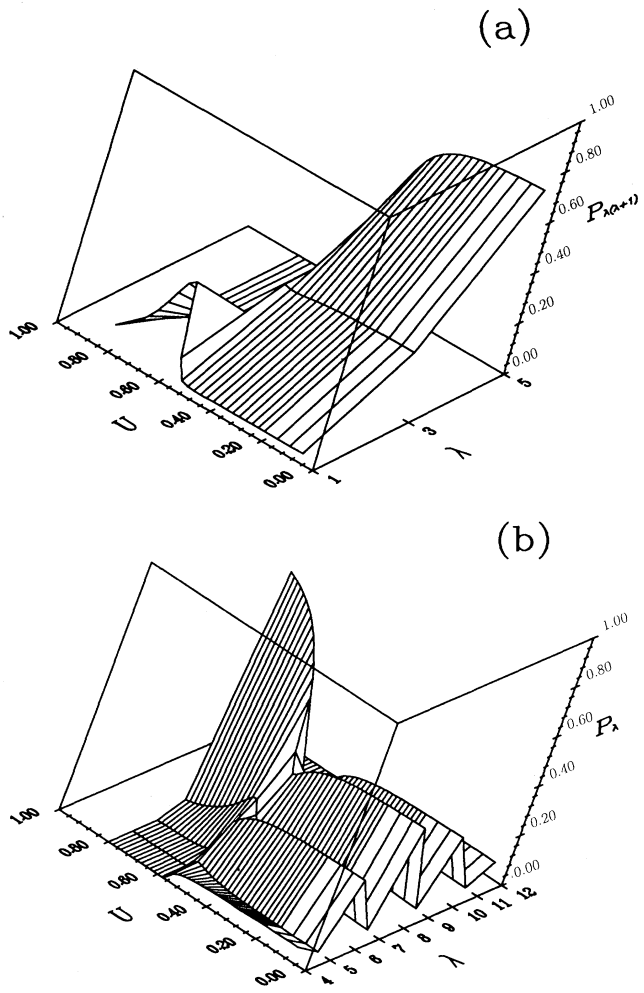

FIG. 5. (a) The ten-site $P_{|\Delta|^2}(\lambda(\lambda+1))$ for odd λ and (b) the eight-site $P_{O_{\rm CDW}}(\lambda)$ at $t=0.04$ for various U ($0.05\le U\le 0.8$, $V=1.0-U$). Both the bump in (a) and cusp in (b) at $U\sim 0.57$ smoothes out when t changes from 0.03 to 0.05. This implies the first-order transition switches over to a second-order transition at $t/(U+V)\sim 0.04\pm 0.01$.

Physically, the "pair twist" boundary condition is equivalent to joining the ends of the one-dimensional chain to form a loop encircling a suitable magnetic flux.

To reuse the code designed for periodic boundary conditions, we apply a canonical transform $c^{\dagger}_{i,\sigma} \rightarrow e^{i\phi_p/N} c^{\dagger}_{i,\sigma}$ in case (3.1a) and $c^{\dagger}_{i,\sigma} \rightarrow e^{i\phi_s \sigma/N} c^{\dagger}_{i,\sigma}$ in case (3.1b). This will reduce the awkward boundary condition back to a periodic one with H transformed to

$$H \rightarrow -\sum_{i,\eta=\pm 1,\sigma} (te^{i\phi_p \eta/N} c^{\dagger}_{i+\eta\sigma} c_{i\sigma} + Ve^{i2\phi_p \eta/N} c^{\dagger}_{i+\eta\uparrow} c^{\dagger}_{i+\eta\downarrow} c_{i\downarrow} c_{i\uparrow}) + \sum_i U n_{i\uparrow} n_{i\downarrow} , \tag{3.2a}$$

$$H \rightarrow -\sum_{i,\eta=\pm 1,\sigma} (te^{i\phi_s \sigma\eta/N} c^{\dagger}_{i+\eta\sigma} c_{i\sigma} + Vc^{\dagger}_{i+\eta\uparrow} c^{\dagger}_{i+\eta\downarrow} c_{i\downarrow} c_{i\uparrow}) + \sum_i U n_{i\uparrow} n_{i\downarrow} \tag{3.2b}$$

for pair and spin twists, respectively.

In Fig. 7 we have plotted $(N/t)|E_{K=0}(\phi_p=\pi) - E_{K=0}(\phi_p=0)|$, the differences of the scaled ground-state energies for the momentum $K=0$ sector calculated with and without a spin twist $\phi_s=\pi$, versus U ($V=1.0-U$) for various $t(0.01 \le t \le 1.0)$ at $N=10$. There are several facts worth mentioning. First, for $t=0$ and $U/(U+V)<0.57$ where the ground state consists purely of freely moving pairs, no spin degree of freedom exists in the ground state and

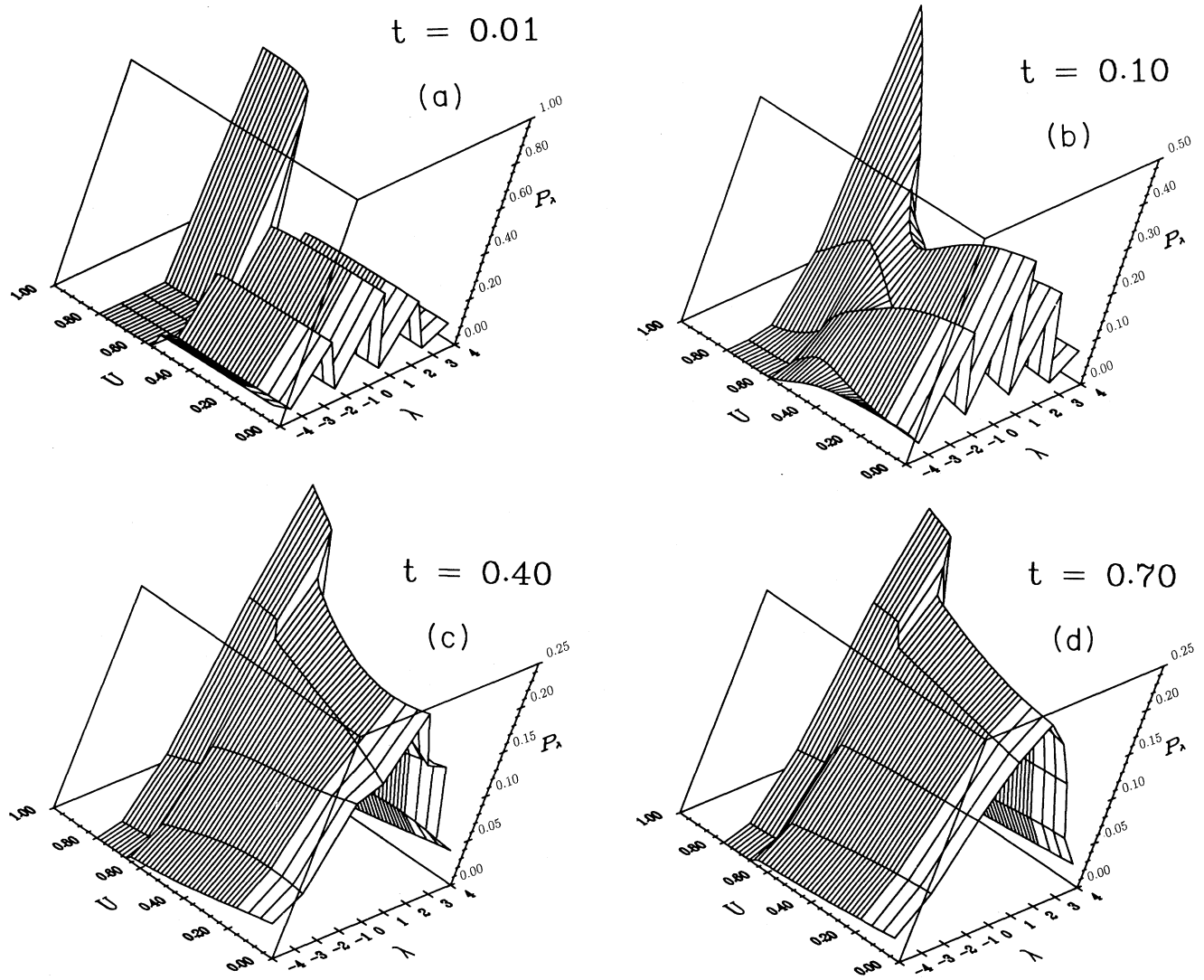

FIG. 6. The eight-site eigenprojection decomposition $P_{O_{\rm CDW}}(\lambda)$ for the charge-density-wave operator $\hat{O}_{\rm CDW}$ at $t=$(a) 0.01, (b) 0.10, (c) 0.40, and (d) 0.70. We have plotted them with different scales in order to bring out various features. First, there is always a discontinuity in $\partial P_{O_{\rm CDW}}(0)/\partial U$ at $U \sim 0.60 \pm 0.05$ which moves towards bigger U as we increase t. Second, in the small-U side of the phase diagram, there is a very strong even-odd dependence in λ of $P_{O_{\rm CDW}}(\lambda)$ for small t which goes away at $t \sim 0.7$.

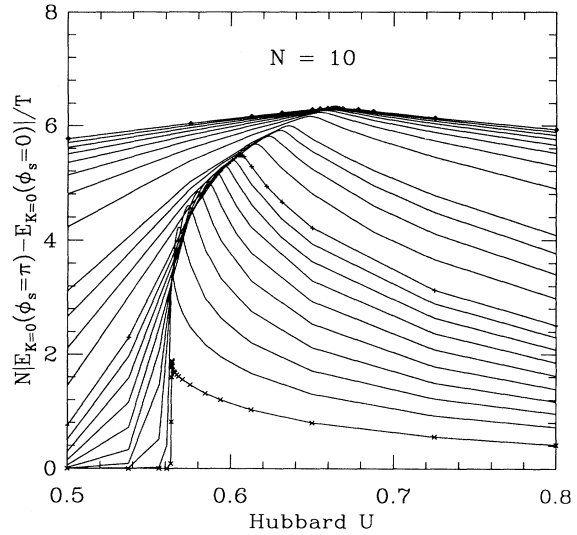

FIG. 7. The differences between the scaled ground-state energies for the momentum $K=0$ sector calculated with and without a spin twist, $(N/t)|E_{K=0}(\phi_s=\pi)-E_{K=0}(\phi_s=0)|$ for $N=10$ and various t $(0.01\leq t\leq 1.00)$. The crosses, plusses, and diamonds correspond to $t=0.01$, 0.1, and 1.0, respectively. The corresponding graphs for $N=6,8$ is quantitatively very similar to the $N=10$ case.

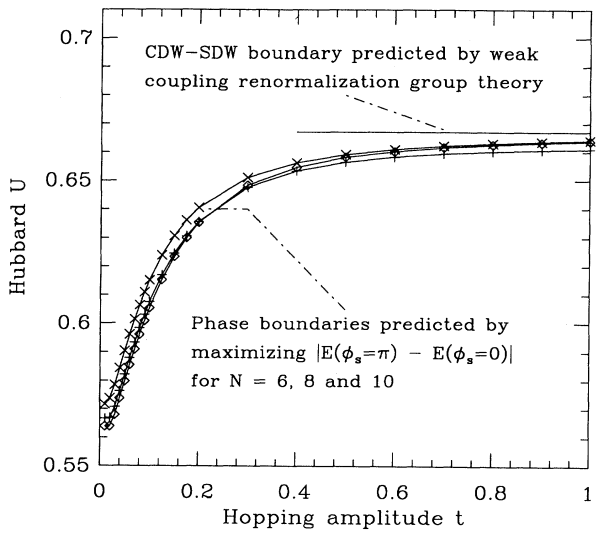

FIG. 8. Trajectories of the position of the "cusp" in $(N/t)|E_{K=0}(\phi_s=\pi)-E_{K=0}(\phi_s=0)|$ for $0.01\leq t\leq 1.0$, $V=1.0$ $-U$ at various sample sizes $N=6,8,10$. Notice they overlap on top of each other within 1% and converge to $U\sim\frac{2}{3}$ as we increase t. This is consistent with the value for the CDW-SDW transition predicted by the renormalization-group analysis in the weak-coupling limit.

$(N/t)|E_{K=0}(\phi_s=\pi)-E_{K=0}(\phi_s=0)|\equiv 0$ as expected. Second, if we plot the same set of curves for $N=6$ and 8, they are strikingly similar to Fig. 7 despite the apparent differences in the corresponding single particle and pair gaps, ΔE_{single} and ΔE_{pair}, as shown in Fig. 2. Third, a cusp originates at $U\sim 0.57$ for $t\sim 0.1$ and moves towards $U\sim 0.67$ for larger t. Since $(N/t)|E_{K=0}(\phi_s=\pi)-E_{K=0}(\phi_s=0)|$ is singular at that cusp for small t, the position of the cusp should correspond to one of the phase boundaries, up to finite-size corrections. Finally, if we plot such trajectories for $N=6,8,10$ as shown in Fig. 8, we see they overlap each other to within 1%. Combining these facts and remembering that in the weak-coupling limit ($t\gg U,V$) we expect a CDW-SDW transition line at $U\sim 2V \Longleftrightarrow U/(U+V)\sim 0.67$, we believe the trajectory of this cusp corresponds to the CDW-SDW phase boundary.[9]

Another possible application of the twisted boundary condition is to study the effect of the pair and spin twist on the expectation values of the eigenprojection operators like $P_{O_{SC}}$ and $P_{|\Delta|^2}$ we have discussed before. For general parameters, the physics is determined by several competing factors from the pairs and other charge or spin excitations. Since the spin and pair twist couple them in different manner, we can use the dependence of P_O on ϕ_p and ϕ_s to infer which factor dominates the physics. In Fig. 9 we have shown $P_{|\Delta|^2}(\lambda(\lambda+1))$ calculated under various boundary conditions [periodic in Fig. 9(a), $\phi_p=\pi$ in Fig. 9(b), and $\phi_s=\pi$ in Fig. 9(c)] for the maximum possible $\lambda=\lambda_{\max}=4$ at $N=8$. When we apply pair twist to the system, $P_{|\Delta|^2}(\lambda_{\max}(\lambda_{\max}+1))$ is strongly suppressed for $U\leq 0.57$. In contrast, when we apply spin twist to the system, $P_{|\Delta|^2}(\lambda_{\max}(\lambda_{\max}+1))$ is only slightly disturbed. This implies the existence of a small U phase whose behavior is dominated by pairs. Also, it is obvious when the spin twist ϕ_s varies from π to 0, $P_{|\Delta|^2}(\lambda_{\max}(\lambda_{\max}+1))$ is strongly suppressed for U above some t-dependent value between 0.57 and 0.67. This indicates there is also a large-U phase whose physics is dominated by spin. All this is clearly consistent with our heuristic expectation of the phase diagram discussed in Sec. II B.

IV. RENORMALIZATION-GROUP ANALYSIS

A. Derivation

In order to understand the conflicts between the numerical results of Penson and Kolb[1] and the renormalization-group analysis of Affleck and Marston[2] concerning the phase transition at $(t:U:V)\sim(1.0:0:1.4)$, let us compare our numerical results with predictions from the renormalization-group (RG) equations for weakly coupled 1D Fermi gas at half filling. Given the PKH Hamiltonian H, and the fact $\mu=U/2$ at half filling, we can rewrite $H-\mu N$, up to a constant, as

$$:-\sum_{i,\eta=\pm 1}\left[\tilde{t}\sum_{\sigma}c^{\dagger}_{i+\eta\sigma}c_{i\sigma}+V\Delta^{\dagger}_{i+\eta}\Delta_i\right]+U\sum_i n_{i\uparrow}n_{i\downarrow}:\ ,$$

where $\tilde{t}=t+(V/\pi)$ and :: denote normal ordering with respect to the ground state of $-t\sum_{i,\eta,\sigma}c^{\dagger}_{i+\eta\sigma}c_{i\sigma}=-t\sum_{k,\sigma}\cos(k)c^{\dagger}_{k\sigma}c_{k\sigma}$. Using this, we can convert the partition function to a functional integral,

$$\mathcal{Z}=\int \mathcal{D}[c^{\dagger},c]\exp\left\{-\int d\tau \sum_i \left[\sum_\eta [c^{\dagger}_{i+\eta}(\tilde{\partial}-\tilde{t})c_i - V\Delta^{\dagger}_{i+\eta}\Delta_i]+Un_{i\uparrow}n_{i\downarrow}\right]\right\},$$

where $\tilde{\partial}$ is regularized in such a way that the contributions from all self-interacting diagrams vanish.

To connect this functional integral with continuum RG equations, we have to separate those contributions in $\mathcal{Z}$ originating from degrees of freedom with nonlinear dispersion relations. This is because continuum RG equations rely on the scaling hypothesis which is no longer valid for such degrees of freedom.

In theory, we pick an arbitrary $\delta<\pi/2$, small enough such that over the range $||k|-(\pi/2)|<\delta$ the dispersion relation is approximately linear. We then integrate away the "fast" modes (i.e., those $c^{\dagger}_k, c_k$ satisfying $||k|-(\pi/2)|>\delta$) and reexpress the partition function $\mathcal{Z}$ in terms of an δ-dependent effective action S^{δ}_{eff} which involves only the "slow" modes,

$$\mathcal{Z}=\int \mathcal{D}[c^{\dagger}_{\text{slow}},c_{\text{slow}}]\exp\{-S^{\delta}_{\text{eff}}(c^{\dagger}_{\text{slow}},c_{\text{slow}})\}\ .$$

We then expand $S^{\delta}_{\text{eff}}=(1/2!)\Gamma^{\delta}_2\hat{c}\,\hat{c}+(1/4!)\Gamma^{\delta}_4\hat{c}\,\hat{c}\,\hat{c}\,\hat{c}+\cdots$ as a "polynomial" in $\hat{c}=c^{\dagger}_{\text{slow}}$ or c_{slow} and identify $\Gamma^{\delta}_{4,k_i=\pm\pi/2,\omega_i=0}$ with the running coupling coefficients in the RG equations at cutoff δ. We then use the continu-

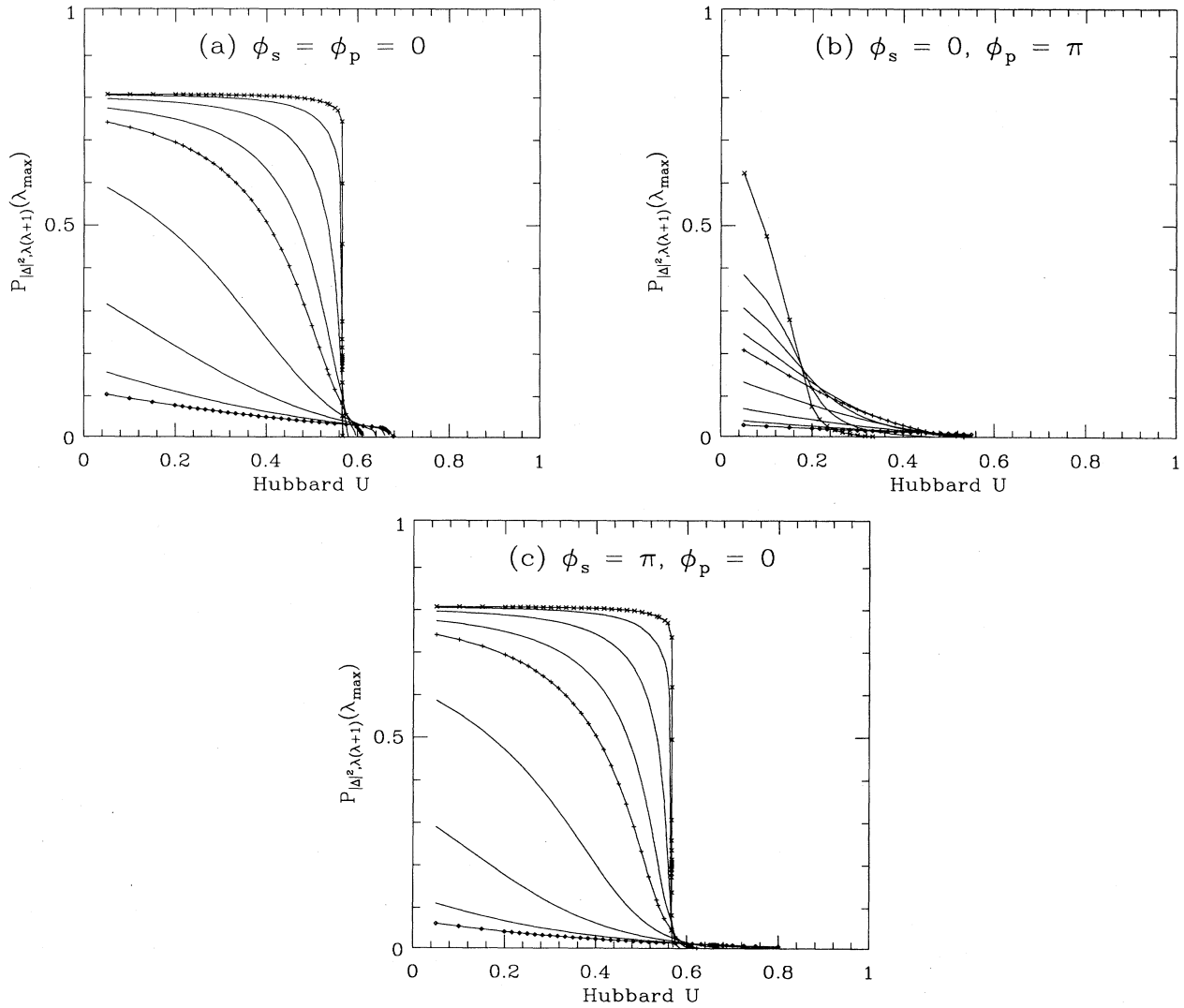

FIG. 9. The $\lambda=\lambda_{\max}=4$ component of the eight-site eigenprojection decomposition $P_{|\Delta|^2}(\lambda(\lambda+1))$ vs U ($0.05\le U\le 0.8$) for various t ($0.01\le t\le 1.00$) calculated under different boundary conditions—periodic in (a), $\phi_p=\pi$ in (b), and $\phi_s=\pi$ in (c). The crosses, pluses, and diamonds correspond to $t=0.01$, 0.1, and 1.0, respectively.

um RG equations to approximate the limiting behavior of S^{δ}_{eff} as $\delta \searrow 0$ and infer the "long-wavelength" physics of the system.

The lowest-order approximation of S^{δ}_{eff} can be calculated by integrating the fast modes in the standard manner as outlined in Ref. 2. It turns out Γ^{δ}_2 remains invariant and when we express $\Gamma^{\delta}_{4,|k_i|=\pi/2,\omega_i=0}$ in terms of the g_1, g_2, g_3, g_4 defined in Ref. 10, the nonvanishing running coupling constants are given by

$$g_{1\parallel}=g_{1\perp}=g_1=(U-2V)+\frac{1}{2\pi\tilde{t}}(U-2V)^2\ln\tan\left[\frac{\delta}{2}\right], \tag{4.1a}$$

$$g_{2\parallel}=g_{2\perp}=g_2=(U-2V) -\frac{1}{2\pi\tilde{t}}\left[4UV\ln\tan\left[\frac{\delta}{2}\right]+4V^2(1-\sin\delta)\right], \tag{4.1b}$$

$$g_{3\perp}=g_3=(U+2V)+\frac{1}{2\pi\tilde{t}}\left[(4V^2-U^2)\ln\tan\left[\frac{\delta}{2}\right] +4V^2(1-\sin\delta)\right], \tag{4.1c}$$

$$g_{4\perp}=g_4=(U+2V), \tag{4.1d}$$

$$g_{3\parallel}=g_{4\parallel}=0. \tag{4.1e}$$

This is basically what Affleck and Marston derived in Ref. 2 except we do not assume $\delta \ll \pi/2$ here.

Setting $2\pi\tilde{t}$ to 1, we than supply Eqs. (4.1a)–(4.1d) as initial conditions to the following two-loop continuum-limit RG equations[10] in $y=-\ln(\delta/2)$,

$$-dg_s/dy=g_s^2+\tfrac{1}{2}(g_s+g_4)g_s^2, \tag{4.2a}$$

$$-dg_\rho/dy=g_3^2+\tfrac{1}{2}(g_\rho-g_4)g_3^2, \tag{4.2b}$$

$$-dg_3/dy=g_\rho g_3+\tfrac{1}{4}(g_\rho^2+g_3^2-2g_\rho g_4)g_3, \tag{4.2c}$$

$$-dg_4/dy=\tfrac{3}{4}(g_\rho g_3^2-g_s^3), \tag{4.2d}$$

where $g_\rho := g_1-2g_2$ and $g_s := g_1$. Figure 1 shows the result for a typical $\delta=0.02$ when we integrate Eqs. (4.2a)–(4.2d) to $y\to\infty$.

The phase diagram is composed of five regions characterized by the limiting values of the renormalized couplings,

$$tABC:\ g_s=g_3=0,\ g_4\sim 2.5,\ g_\rho \lesssim 0,$$

$$tCDE:\ g_s=g_\rho-g_3=-2,\ g_4=0,$$

$$tEP:\ g_s=g_3=0,\ g_4\sim -2.5,\ g_\rho \gtrsim 0,$$

$$UBA:\ g_s=g_\rho=g_3=-2,\ g_4=0,$$

$$VPED:\ g_s=g_\rho=g_3=-2,\ g_4=0.$$

Within the current level of approximation, the renormalization-group analysis poses several uncertainties in its quantitative predictions. For example, if we vary δ, the precise positions of various transition points change. The limiting values of the renormalized couplings also depend on how we handle the g_4 term. We may choose to absorb it into the "unperturbed Hamiltonian" and physically, this will lead to a renormalization of the Fermi velocities. However, the qualitative features of the phase diagram remain invariant under all these changes.

B. Comparison with results from exact diagonalization

Based on our numerical results at $t/V\sim 0.7\pm 0.1$ along the tV line, we identify the point P with the parameters $t:U:V=$ 0.7:0.0:1.0. Within the current level of approximation, this corresponds to the choice of $\delta\sim 2\exp(-2.5-0.7\pi)\sim 0.02$. If we overlay Fig. 1 with our results from exact diagonalization, the second-order CDW-SDW transition line (the circles in Fig. 1) from exact diagonalization matches nicely with its RG prediction $tC(U=2V)$ for small t. We have also estimated the position of the CDW-SC transition line by minimizing the expression

$$\frac{1}{6}\sum_\lambda[P_{O_{\text{CDW}}}(\lambda+1)-2P_{O_{\text{CDW}}}(\lambda)+P_{O_{\text{CDW}}}(\lambda-1)]^2$$

for $N=10$ and 12. They predict a phase boundary (the squares and diamonds in Fig. 1) qualitatively similar to their renormalization-group counterpart DE. However, there are a few qualitative inconsistencies between the renormalization-group analysis and the results from exact diagonalization.

First, we have not been able to observe the phase boundaries tE and AB predicted by RG equations in our exact diagonalization. The phase boundary tE lies purely in the weak-coupling regime where the RG equation can be trusted. tE should have been visible had we chosen the correct order parameter to use in the spectral decomposition. Since no transition takes place along the tU line at "exactly" half filling[3] and AB lies purely in the intermediate- and strong-coupling regimes where RG analysis is unreliable, we believe AB is simply an artifact.

Second, inconsistencies come in when we try to map our phase diagram to that of a weakly interacting Fermi gas. Using the classification given in Ref. 10, we may infer several conclusions: in phase tUC there is a gap in the charge but not in the spin sector and the system is in a SDW state; in phase $tCDE$, there is a gap in both the spin and charge sector, but since CDW is the dominant instability, the system should be in a CDW state. This view is consistent with our observations of the CDW order parameter in exact diagonalization. The same classification also leads to the conclusion that in phase tEP, there is a gap in the spin but not in the charge sector and the system is superconducting. In phase $VPED$, only the CDW response functions can diverge and the system can only be in a CDW state. The last conclusion is totally against physical intuition. The following argument shows that it is definitely wrong. Along the UV line for $U<(4/\pi)V$, the system is equivalent to the XY model and we can calculate the equal time (singlet)–superconducting response functions and the charge-charge correlation functions exactly.[11] They are given by

$$\langle \Delta_x^\dagger \Delta_0 \rangle = \frac{1}{2} \prod_{j=1}^{[x/2]-1} \left[1-\frac{1}{4j^2}\right]^j \prod_{j=1}^{[x/2]-1} \left[1-\frac{1}{4j^2}\right]^j \sim O(x^{-1/2}) , \quad (4.3)$$

$$\langle (n-1)_x (n-1)_0 \rangle = \delta_{x0} + 2[1-(-1)^x](\pi x)^{-2} \sim O(x^{-2}) . \quad (4.4)$$

Since the oscillating part of the charge-charge correlation function is the CDW response function and it decays much faster then the superconducting one, phase *VPED* is really in a superconducting instead of a CDW state.

Finally, let us compare our results with the analysis of Affleck and Marston.[2] Figure 10 illustrates schematically the V dependence of the running coupling constants g_ρ and g_3 (Ref. 12) at fixed cutoff δ along the tV line. As V increases from 0, the running coupling constants move away from the separatrix $g_\rho = |g_3|$, and for small positive V, the corresponding renormalization-group trajectory terminates on the critical line $g_3 = 0$ at $g_\rho \sim 4(V^3/2\pi\tilde{t})^{1/2}\exp(-\pi\tilde{t}/4V)$. This renormalizes the dispersion relation of the lowest-lying charge-density-wave excitations slightly but leaves the charge sector gapless.[13] As pointed out to us by Affleck,[14] the low-energy sector of the PKH model in the large-V regime is equivalent to the XXZ model with a small repulsive zz coupling. This is well known to be a strictly marginal perturbation which changes the exponents but leaves the charge sector gapless. Given that the charge sector is gapless for both small and large V, Affleck and Marston then argued that it should remain gapless for all V and inferred that there is no transition along the tV line.[2]

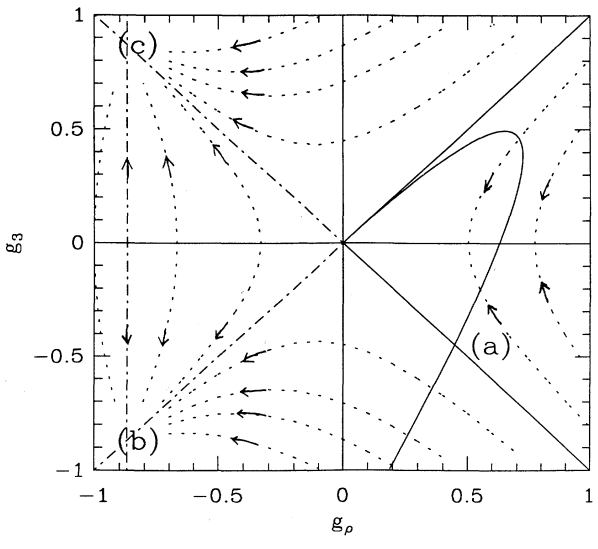

FIG. 10. Illustration of the V dependence of the running coupling constants g_ρ and g_3 at fixed cutoff $\delta = 0.02$ along the tV line. The dashed curves are schematic sketches of the renormalization-group trajectories. The solid curve is the running coupling constants we calculated using Eq. (4.1a) at $\delta = 0.02$. Presumably when V increases beyond $1.4t$, it crosses the lower separatrix $g_3 = -g_\rho < 0$ (a) and the system will be renormalized to the lower Luther-Emery fixpoint (b) as shown.

However, this conclusion is inconsistent with the observed qualitative differences in $P_{O_{\rm CDW}}$ for large and small V and the apparent crossing of the small and large V behavior at $V/t \sim 1.4$ as depicted in Fig. 6. Furthermore, our RG calculations show that for intermediate V, the momentum dependence in the dispersion relation of the pairs can drive the running coupling constants at fixed cutoff δ across the lower branch of the separatrix. g_ρ, g_3 will then renormalize into their limiting strong-coupling values. This will in turn favor the formation of a gap in the charge excitation spectrum. Combining these hints, we propose the following scenario.

In the weak-coupling limit, the charge sector consists of excitations which do not care whether or not a site is singly occupied. As we increase V beyond $1.4t$, a gap opens up for those charge excitations with a projection on singly occupied sites. However, excitations involving no unpaired electrons (i.e., all the sites involved will be either empty or doubly occupied) remain gapless. We expect them to be the gapless excitations required by gauge symmetry arguments in the absence of the long-range Coulomb interactions. As a result, the low-energy charge sector in the large-V limit consists solely of such pair fluctuations which are analogous to the Bogoliubov-Anderson modes in the usual BCS superconducting theory.

In essence, we believe that the Penson-Kolb transition is characterized by the opening of a single-particle excitation gap at $V \sim 1.4t$.

V. SUMMARY AND FUTURE DIRECTIONS

We have proposed the Penson-Kolb-Hubbard model as a phenomenological model which captures some of the essential physics of the high-T_c materials and have studied the ground-state phase diagram of its one-dimensional counterpart both by exact diagonalization using the Lanczos algorithm and by renormalization-group equations. Due to the sample-size dependence of period 4 in numerical data, we have abandoned the standard approach of studying energy gaps and correlation functions. Instead, we look at the expectation values of the eigenprojection operators associated with the CDW and superconducting order parameters. Augmented with studies based on the idea of twisting the boundary conditions, we have confirmed various features of the phase diagram which we predicted through heuristic arguments. Unlike the data we collected through energy-level analysis, these techniques produce results much less sensitive to changes in sample size. In addition, when used with the "correct" order parameter, the expectation values of the eigenprojection operators offer distinctive features right at the transition points. This allows us to determine the transition lines accurately using only calculations with very small samples. In conclusion, these techniques provide a nice framework to visualize what is happening physically. They allow us to avoid expensive large-N calculations[15] and still understand the underlying physics.

On the other hand, our renormalization-group analysis is far from perfect and poses certain uncertainties in its

predictions. The breakdown of the "qualitative" predictions of continuum-limit RG equations in the intermediate-coupling regime is particularly worrisome. This indicates that as we increase the couplings, the "momentum" dependence of the coupling is no longer irrelevant and hence RG equations constructed in the continuum limit completely lose their predictive power for intermediate couplings. A possible improvement would be reanalyzing the problem using a renormalization scenario which adheres closer to Wilson's original idea of momentum-shell recursion and keeps the "momentum" dependence at all times. Some work is in progress along this direction and preliminary results look promising. It would also be interesting to repeat the current study on the two-dimensional version of the PKH model and compare it with experimental data on the cuprates whose physics is believed to be quite two-dimensional in nature.

ACKNOWLEDGMENTS

This work is supported by the NSF-MRL program administrated by the Center for Materials Research at Stanford University. We would like to thank Edward Rezayi, S. C. Zhang, Castor Fu, and J. B. Marston for useful conversations and Ian Affleck for helpful criticism.

[1]K. A. Penson and M. Kolb, Phys. Rev. B **33**, 1663 (1986); M. Kolb, K. A. Penson, J. Stat. Phys. **44**, 129 (1986).

[2]Ian Affleck and J. Brad Marston, J. Phys. C **21**, 2511 (1988).

[3]Elliott H. Lieb and F. Y. Wu, Phys. Rev. Lett. **20**, 1445 (1968).

[4]J. Cullum and R. A. Willoughby, *Lanczos Algorithms for Large Symmetric Eigenvalue Computations* (Birkhauser, Basel, 1985), Vols. 1 (theory) and 2 (programs).

[5]J. W. Cannon, R. T. Scalettar, and E. Fradkin, Phys. Rev. B **44**, 5995 (1991).

[6]E. Gagliano, E. Dagotto, A. Moreo, and F. Alcaraz, Phys. Rev. B **34**, 1677 (1986).

[7]The Lanczos algorithm is a "memory bounded" algorithm. In order to minimize the amount of memory required, we perform all our calculations using basic vectors of fixed particle number.

[8]M. E. Fisher, M. B. Barber, and D. Jasnow, Phys. Rev. A **8**, 1111 (1973).

[9]We have repeated the analysis using the differences of scaled ground-state energies over all momentum sectors with and without a π-spin or π-pair twist and we have located the same set of boundaries.

[10]J. Sólyom, Adv. Phys. **28**, 201 (1979).

[11]E. Lieb, T. Schultz, and D. Mattis, Ann. Phys. (N.Y.) **16**, 407 (1961).

[12]g_ρ and g_3 corresponds to $2\lambda_1$ and $-4\lambda_3$ in Ref. 2.

[13]I. Affleck, in *Fields, Strings and Critical Phenomena,* Proceedings of Les Houches Summer School of Theoretical Physics, Haute-Savoie, France, 1988, edited by E. Brezin and J. Zinn-Justin (North-Holland, Amsterdam, 1990), pp. 563–640.

[14]I. Affleck (private communication).

[15]There are other technical advantages of using the eigenprojection decompositions and the twisted boundary conditions over canonical energy-level analysis. Both the eigenprojection decomposition and the twisted boundary conditions only require the knowledge of the ground state of the system. We can apply a special version of the Lanczos algorithm (Ref. 6) which typically runs 30 times faster than the full blown version (Ref. 4) needed in an energy-level analysis.